Prediction of Electron-Transfer Reactivities from Contemporary Theory: Unified Comparisons for Electrochemical and Homogeneous Reactions

Joseph T. Hupp and Michael J. Weaver*

Department of Chemistry, Purdue University, West Lafayette, Indiana 47907 *(Received: February 4, 1985)*

Suitable theoretical formalisms are outlined for examining and predicting rate parameters for outer-sphere electron transfer in heterogeneous and homogeneous environments on a unified basis. They are utilized to calculate rate constants and activation parameters for 11 electrochemical and 45 homogeneous self-exchange and cross reactions involving transition-metal aquo, ammine, ethylenediamine, and polypyridine redox couples from the appropriate structural and thermodynamic data. Comparison between the calculated and experimental work-corrected rate constants, k_{calcd} and k_{cor}, respectively, indicates that almost uniformly $k_{calcd} \gtrsim k_{cor}$, the latter values being typically ca. 10–10^3-fold smaller. These rate discrepancies are reflected chiefly in the activation entropies, although partly compensated by differences between the experimental and calculated activation enthalpies. Although the values of k_{calcd}/k_{cor} depend somewhat upon the reaction environment as determined by the nature of the coordinated ligands and the metal surface, they are approximately independent of the magnitude of k_{cor} or the driving force. Taken together, these findings suggest tht the major origin of the discrepancies between k_{calcd} and k_{cor} is associated with changes in local solvent structure when forming the precursor state. Nonadiabaticity may contribute importantly by necessitating that the reacting centers be in very close proximity. Reactions at "hydrophilic" metal surfaces, such as lead and gallium, that are known to strongly adsorb water molecules yield remarkably similar theory–experiment disparities to those seen with cationic coreactants in homogeneous solution. The markedly closer agreement obtained for some reactions at mercury is attributed to the relatively mild perturbation exerted by this metal surface upon the local solvent structure.

Understanding the structural and thermodynamic factors that influence rate parameters for outer-sphere electron-transfer reactions is a problem of widespread interest to experimental kineticists and theoreticians alike.[1] Besides the well-known reactions of this type involving pairs of transition-metal complexes in homogeneous solution, another important class is provided by related electrochemical processes, i.e., where one redox couple is replaced by an electrode surface. We have a particular interest in the latter type; a major objective is to develop a unified understanding of the factors that control the kinetics of electrochemical reactions in comparison with those that influence homogeneous processes.[2-8] The seminal work of Marcus established that straightforward relationships are expected between the rate constants for corresponding self-exchange and cross reactions in homogeneous solution, and also with the corresponding electrochemical reactions at metal surfaces.[9] Since then a great deal of attention has been devoted to testing the applicability of the former relationships,[10-12] and some (albeit more limited) scrutiny of the latter.[2,4] Broadly speaking, reasonable agreement with experimental data has been obtained, even though noticeable discrepancies are often observed for reactions having moderate or large driving forces.[10,11]

Although useful, such "relative rate" predictions[10a] are inherently limited as a test of the underlying theoretical models due to the extensive cancellation of terms that is inevitably involved. A more demanding test of electron-transfer models involves their ability to predict rate parameters for individual reations. Such "absolute rate" comparisons[10a] have been relatively sparse.[8,13,14] This has been due primarily to the paucity of the bond length and vibrational data that are necessary in order to calculate the Franck–Condon barriers. However, bond distance data have recently been obtained for a number of simple transition-metal redox couples from solution EXAFS as well as X-ray crystallographic measurements,[14] and appropriate vibrational data are becoming available in many cases from Raman as well as infrared spectroscopy.[15,16] These structural data have recently been utilized to calculate rate constants for several homogeneous self-exchange reactions.[14]

It is clearly desirable to extend such individual absolute rate comparisons between theory and experiment to encompass homogeneous cross reactions and electrochemical processes. These reactions form the bulk of systems for which quantitative outer-sphere rate parameters have been gathered, providing a rich body of experimental data. Such comparisons should therefore enable the ability of theory for describing outer-sphere kinetics to be tested for a variety of reaction environments and thermodynamic driving forces. Theory–experiment comparisons for homogeneous cross reactions have been made via the self-exchange rate parameters inferred for the parent redox couples by using the Marcus cross relationships.[4,5] Although maintaining the same theoretical format as that employed for self-exchange processes, this procedure has the disadvantage of being subject to the various approximations embodied in the theoretical derivation of the cross relationship.[9] However, absolute rate comparisons between theory and experiment may be made directly for cross, as well as for self-exchange, reactions provided that thermodynamic and structural data are available for both redox couples.[17]

Electrochemical reactions have for the most part been dealt with separately, and seldom with the degree of insight and so-

(1) For recent reviews, see: (a) Schmidt, P. P. "Specialist Periodical Report: Electrochemistry"; The Chemical Society: London, 1975; Vol. 5, Chapter 2; 1977, Vol. 6, Chapter 4. (b) Cannon, R. D. "Electron Transfer Reactions"; Butterworths: London, 1980. (c) Newton, M. D. *Int. J. Quantum Chem. Quantum Chem. Symp.* **1980**, *14*, 363. (d) Sutin, N. *Prog. Inorg. Chem.* **1983**, *30*, 441. (e) Newton, M. D.; Sutin, N. *Annu. Rev. Phys. Chem.* **1984**, *35*, 437.

(2) Weaver, M. J. *J. Phys. Chem.* **1980**, *84*, 568.

(3) Weaver, M. J.; Tyma, P. D.; Nettles, S. M.; *J. Electroanal. Chem.* **1980**, *114*, 53.

(4) Weaver, M. J.; Hupp, J. T. *ACS Symp. Ser.* **1982**, *No. 198*, 181.

(5) Hupp, J. T.; Weaver, M. J. *Inorg. Chem.* **1983**, *22*, 2557.

(6) Weaver, M. J.; Li, T. T.-T. *J. Phys. Chem.* **1983**, *87*, 1153.

(7) Hupp, J. T.; Weaver, M. J. *J. Phys. Chem.* **1984**, *88*, 1463.

(8) Hupp, J. T.; Liu, H. Y.; Farmer, J. K.; Gennett, T.; Weaver, M. J. *J. Electroanal. Chem.* **1984**, *168*, 313.

(9) (a) Marcus, R. A. *J. Phys. Chem.* **1963**, *67*, 853. (b) Marcus, R. A. *J. Chem. Phys.* **1965**, *45*, 679.

(10) For example see: (a) Bennett, L. E. *Prog. Inorg. Chem.* **1973**, *18*, 1. (b) Sutin, N. *Inorg. Biochem.* **1973**, Chapter 19. (c) Linck, R. G. *Surv. Prog. Chem.* **1976**, *7*, 89.

(11) Chou, M.; Creutz, C.; Sutin, N. *J. Am. Chem. Soc.* **1977**, *99*, 5615.

(12) Weaver, M. J.; Yee, E. L. *Inorg. Chem.* **1980**, *19*, 1936.

(13) Endicott, J. F.; Durham, B.; Glick, M. D.; Anderson, T. J.; Kuszaj, J. M.; Schmousees, W. G.; Balakrishnan, K. P. *J. Am. Chem. Soc.* **1981**, *103*, 1431.

(14) Brunschwig, B. S.; Creutz, C.; MaCartney, D. H.; Sham, T.-K.; Sutin, N. *Faraday Discuss. Chem. Soc.* **1982**, *74*, 113.

(15) (a) Best, S. P.; Beattie, J. K.; Armstrong, R. S. *J. Chem. Soc., Dalton Trans.*, **1984**, 2611. (b) Jenkins, T. E.; Lewis, J. *Spectrochim. Acta* **1981**, *37A*, 47. (c) Bernhard, P.; Ludi, A. *Inorg. Chem.* **1984**, *23*, 870.

(16) (a) Schmidt, K. H.; Muller, A. *Inorg. Chem.* **1975**, *14*, 2183; (b) *Coord. Chem. Re.* **1976**, *19*, 41.

(17) Siders, P.; Marcus, R. A. *J. Am. Chem. Soc.* **1981**, *103*, 741.

0022-3654/85/2089-2795$01.50/0

phistication that has been afforded to homogeneous processes. This is unfortunate since, besides the practical importance of electrochemical processes, they enable the reaction energetics for a *single* reacting species to be assessed directly as a function of driving force. Moreover, electrochemical and homogeneous cross reactions are closely related in that they both involve widely varying reaction thermodynamics and feature chemically dissimilar reaction partners whose structure can be widely varied. Indeed, electrochemical reactions can usefully be perceived as a special type of cross reaction where the metal surface "coreactant" requires no activation and has a continuously variable redox potential.

In this article we outline suitable theoretical formalisms and utilize them to compare experimental rate constants and activation parameters for 11 electrochemical and 45 homogeneous self-exchange and cross reactions with the corresponding parameters calculated from the available structural, vibrational, and redox thermodynamic data. The reactions were chosen on the basis of their structural simplicity and the availability of trustworthy kinetic, structural, and thermodynamic data. They involve spherically symmetric transition-metal M(III)/(II) couples containing aquo, ammine, ethylenediamine, or polypyridine ligands in aqueous solution. The electrochemical rate parameters were obtained in our laboratory, under conditions where electrostatic work-term corrections can be applied quantitatively. Such a broad-based unified examination of the idealized theoretical predictions for both homogeneous and electrochemical reactions enables some of the additional complexities that influence the experimental rate parameters in heterogeneous and homogeneous environments to be identified and their importance assessed.

Theoretical Treatment

(I) Rate Constants. Prior to presenting comparisons between the experimental and theoretical rate parameters, we shall outline the calculational procedures utilized here in order to clarify the underlying physical assumptions. We consider one-electron outer-sphere electrochemical and homogeneous reactions as depicted schematically in eq 1a and 1b, respectively. Both these

$$Ox_1 + e^-[\text{electrode}, (E - E^\circ)] \rightleftharpoons Red_1 \quad (1a)$$

$$Ox_1 + Red_2 \rightleftharpoons Red_1 + Ox_2 \quad (1b)$$

processes can be separated into several distinct steps.[18] Provided that the elementary electron-transfer step is rate determining, the overall observed rate constants k_{obsd} can be expressed as[19-21]

$$k_{ob} = K_p k_{et} \quad (2a)$$

where K_p is the equilibrium constant for forming the precursor state from the separated reactants and k_{et} is the unimolecular rate constant for the electron-transfer step. It is convenient to consider a "electrostatic work-corrected" rate constant, k_{cor}, that would equal k_{obsd} in the absence of Coulombic work terms (vide infra). Approximate values of k_{cor} can be obtained from k_{obsd} for electrochemical or homogeneous reactions by using the Gouy–Chapman[22] or Debye–Huckel[19a,23] models, respectively. Equation 2a can then be written as

$$k_{cor} = K_o k_{et}^{cor} \quad (2b)$$

where K_o and k_{et}^{cor} are the work-corrected values of K_p and k_{et}, respectively.[24] For electrochemical reactions, K_o can be expressed as[21]

$$K_o^e = \delta r_e \quad (3)$$

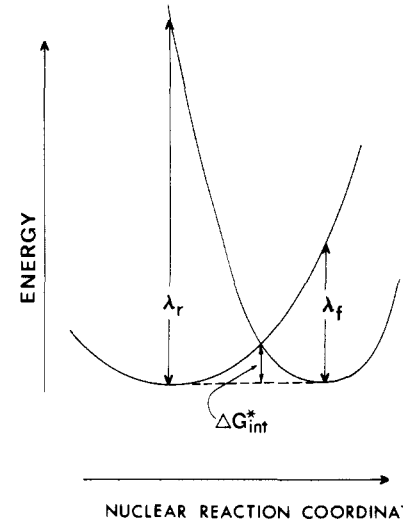

Figure 1. Schematic representation of the forward and reverse reorganization energies, λ_f and λ_r, respectively, and their relationship to the intrinsic barrier, ΔG^*_{int}.

where δr_e is the effective thickness of a reaction zone near the metal surface within which the reactant needs to be located in order to contribute significantly to the overall reaction rate (vide infra). Equation 3 is the heterogeneous analogue of the expression recently employed[14] for K_o for homogeneous reactions, K_o^h, which has the form[19b,25]

$$K_o^h = 4\pi N r_h^2 \delta r_h \quad (4)$$

where N is Avogadro's constant, r_h is the separation distance between the spherical redox centers at their closest approach, and δr_h is the effective reaction zone thickness around either reactant.

An important virtue of the "encounter preequilibrium" approach embodied in eq 2–4 is that it enables the kinetics of both electrochemical and homogeneous reactions to be analyzed on a common basis, involving the unimolecular rate constant k_{et}^{cor}. This quantity can be related to the work-corrected free energy of activation, ΔG^*, by[1c,1d,21,26]

$$k_{et}^{cor} = \nu_n \Gamma_n \kappa_{el} \exp(-\Delta G^*/RT) \quad (5)$$

where ν_n is a nuclear frequency factor (s^{-1}), Γ_n is a nuclear tunneling factor, and κ_{el} is an electronic transmission coefficient.

Equations 2–5 provide a link between the experimental rate data and the "Franck–Condon" barrier, ΔG^*, which is of central significance in electron-transfer theory. The methods used here to calculate ΔG^* in part follow those employed recently by Sutin et al.[14] Thus, we separate ΔG^* into additive contributions arising from the (inner-shell) distortions of the reacting species, ΔG^*_{is}, and the (outer-shell) reorientation of the surrounding solvent, ΔG^*_{os}. However, a key departure from conventionality lies in the method used here to calculate ΔG^*_{is}, prompted in part by our need to evaluate ΔG^*_{is} for electrochemical or cross reactions having moderate or large driving forces. It is usual to calculate ΔG^*_{is} by employing "reduced" force constants, f_r, for the redox couple in place of the individual values associated with bond vibrations in the oxidized and reduced forms, f_{Ox} and f_{Red}.[1d,14] While this procedure is wholly valid for homogeneous self-exchange reactions,[9b] it is not appropriate for cross reactions involving structurally dissimilar redox couples[14,27] nor for electrochemical pro-

(18) Tembe, B. L.; Friedman, H. L.; Newton, M. D. *J. Chem. Phys.* **1982**, *76*, 1490.
(19) (a) Brown, G. M.; Sutin, N. *J. Am. Chem. Soc.* **1979**, *101*, 883. (b) Sutin, N.; Brunschwig, B. S. *ACS Symp. Ser.* **1982**, *198*, 105.
(20) Marcus, R. A. *Int. J. Chem. Kinet.* **1981**, *13*, 865.
(21) Hupp, J. T.; Weaver, M. J. *J. Electroanal. Chem.* **1983**, *152*, 1.
(22) Weaver, M. J. *J. Electroanal. Chem.* **1978**, *93*, 231.
(23) Perlmutter-Hayman, B. *Prog. React. Kinet.* **1971**, *6*, 239.
(24) Although no electrostatic work corrections to k_{et} are required for charge-symmetric homogeneous reactions, generally $k_{et} \neq k_{et}^{cor}$ for reactions where the reactant and product species carry different charges as well as for electrochemical processes since the precursor and successor work terms will be unequal.
(25) (a) North, A. M. "The Collision Theory of Chemical Reactions in Liquids"; Methuen: London, 1964. (b) Levich, V. G. "Advances in Electrochemistry and Electrochemical Engineering"; Interscience: New York, 1966, Vol. 4, p 299.
(26) Brunschwig, B. S.; Logan, J.; Newton, M. D.; Sutin, N. *J. Am. Chem. Soc.* **1980**, *102*, 5978.
(27) Thus, for large driving forces, the barrier height will be determined predominantly by the free-energy profile for the product rather than the reactant species. The use of reduced, rather than individual, force constants under such conditions can commonly yield errors in ΔG^*_{is} of around 1–2 kcal mol^{-1} for the systems considered here.[28]

cesses.[4,28] We have therefore calculated ΔG^*_{is} on the basis of free-energy curves for the individual oxidized and reduced states, using the following procedure.

We employ so-called "intrinsic reorganization parameters",[9b] λ_f and λ_r, for the forward and reverse reactions, respectively. The physical significance of these quantities is shown schematically in Figure 1. They consist of inner-shell components from each reactant, λ_{is}^{Ox} and λ_{is}^{Red}, as well as that from outer-shell reorganization, λ_{os}, such that for the homogeneous reaction 1b

$$\lambda_f = \lambda_{is}^{Ox_1} + \lambda_{is}^{Red_2} + \lambda_{os} \quad (6)$$

$$\lambda_r = \lambda_{is}^{Red_1} + \lambda_{is}^{Ox_2} + \lambda_{os} \quad (7)$$

For electrochemical reactions 1a, $\lambda_{is}^{Red_2} = \lambda_{is}^{Ox_2} = 0$. Generally λ_{is}^{Ox} and λ_{is}^{Red} will differ since $f_{Ox} \neq f_{Red}$. These quantities are related by

$$\lambda_{is} = 0.5\sum f_i(\Delta a)^2 \quad (8)$$

where f_i is the force constant for a given bond which undergoes an alternation in bond length, Δa, between the oxidized and reduced forms.

The required free energy of activation ΔG^* for a given reaction is estimated from the intersection point of the reactant and product free-energy parabolas defined by eq 6–8 for the appropriate driving force, $\Delta G°$. This is obtained from the solution to the relations

$$\Delta G^* = \lambda_f X^2 \quad (9a)$$

where

$$\lambda_f X^2 = \lambda_r(1 - X)^2 + \Delta G° \quad (9b)$$

and X is a dimensionless parameter characterizing the nuclear reaction coordinate.

This approach is only approximate, especially for homogeneous processes. This is because the reactant and product parabolas both consist of several separate contributions, in the latter case from two reacting species; these combine to yield a band of intersection free energies, each corresponding to slightly different nuclear coordinates.[4,30] The lowest, and therefore preferred, free-energy pass generally yields ΔG^*_{is} estimates that are slightly smaller than those obtained from eq 6–8. Fortunately, however, this difference is negligibly small ($\lesssim$0.3 kcal mol^{-1}) for all electrochemical reactions and virtually all cross reactions considered here. Significantly larger differences occur for a few self-exchange reactions having the largest values of ΔG^*_{is}. For these, ΔG^*_{is} was calculated instead by using reduced force constants in order to calculate the minimum ΔG^*_{is}; this approach is correct for the special case of homogeneous self-exchange.[1d]

The outer-shell reorganization energy for electrochemical and homogeneous reactions, λ_{os}^{e} and λ_{os}^{h}, respectively, can be estimated from[9b]

$$\lambda_{os}^{e} = \frac{Ne^2}{2}\left(\frac{1}{a} - \frac{1}{R_e}\right)\left(\frac{1}{\epsilon_{op}} - \frac{1}{\epsilon_s}\right) \quad (10)$$

$$\lambda_{os}^{h} = Ne^2\left(\frac{1}{2a_1} + \frac{1}{2a_2} - \frac{1}{R_h}\right)\left(\frac{1}{\epsilon_{op}} - \frac{1}{\epsilon_s}\right) \quad (11a)$$

where e is the electronic charge, ϵ_{op} and ϵ_s are the optical and static dielectric constants; a, a_1, and a_2 are the appropriate reactant radii; and R_e and R_h are the reactant–image and reactant–reactant distances in the electrochemical and homogeneous reactions, respectively. An alternative to eq 11a is provided by the following relationship[31]

$$\lambda_{os}^{h} = \frac{Ne^2R_h^2}{2l_a^2l_b^2}\left(\frac{1}{\epsilon_{op}} - \frac{1}{\epsilon_s}\right)S \quad (11b)$$

where l_a and l_b are the semimajor and semiminor axes for an ellipsoid encompassing the reactant pair and S is a "shape factor" approximated by $S \approx 1.19 - 0.54e$, where e is the ellipsoid eccentricity. This latter relationship is employed here for calculating λ_{os}^{h} since it can account for ligand interpenetration (vide infra), although a numerical comparison between eq 11a and 11b is given below.

The nuclear frequency factor ν_n is estimated here from[1d]

$$\nu_n = (\nu_{os}^2\Delta G^*_{os} + \nu_{is,1}^2\Delta G^*_{is,1} + \nu_{is,2}^2\Delta G^*_{is,2})/(\Delta G^*_{os} + \Delta G^*_{is}) \quad (12)$$

where ν_{os} is the characteristic frequency of outer-shell (aqueous solvent) reorganization ($\approx 3 \times 10^{12}$ s^{-1}),[32] $\nu_{is,1}$ and $\nu_{is,2}$ are the average vibrational frequencies associated with each reactant couple, and $\Delta G^*_{is,1}$ and $\Delta G^*_{is,2}$ are the corresponding components of ΔG^*_{is} attributable to each reactant. Although conditions favoring a breakdown of the transition-state theory upon which eq 12 is based have been established recently,[32] it should apply under the present circumstances involving moderate or large inner-shell barriers in aqueous media.[32a,c]

An approximate expression for evaluating the nuclear tunneling factor associated with the inner-shell barrier is[1d,33,34]

$$\ln \Gamma_n = \frac{-\Delta H'}{2RT} - \frac{\lambda_{is}}{h\nu_{is}}\left\{\coth\left(\frac{h\nu_{is}}{2k_BT}\right) - \left[\left(\frac{\Delta H'}{\lambda_{is}}\right)^2 + \operatorname{csch}^2\left(\frac{h\nu_{is}}{2k_BT}\right)\right]^{1/2} + \left(\frac{\Delta H'}{\lambda_{is}}\right)\sinh^{-1}\left[\left(\frac{\Delta H'}{\lambda_{is}}\right)\sinh\left(\frac{h\nu_{is}}{2k_BT}\right)\right]\right\} \quad (13)$$

where $\Delta H'$ is the inner-shell part of the enthalpic driving force,[34] k_B is Boltzmann's constant, λ_{is} is the overall inner-shell reorganization energy, and ν_{is} is the average inner-shell vibrational frequency. This relation is applied here to both electrochemical and homogeneous processes. The contribution to Γ_n arising from the outer-shell modes can be neglected due to their lower frequencies. Although eq 12 and 13 utilize mean inner-shell vibrational frequencies for the reactant and product species rather than the individual values employed for calculating the free-energy barrier, this approximation has a negligible influence upon the calculations.

The remaining term in eq 5, κ_{el}, is very difficult to estimate.[1c,34] Instead, following the procedure elsewhere[8,14] we set $\kappa_{el} = 1$, and take the reaction zone thickness, δr_e and δr_h (eq 3, 4), as 0.6 Å. The latter choice is appropriate if the local value of κ_{el} decreases exponentially as the distance between the donor and acceptor sites is increased beyond the point of closest approach.[35] This is

(28) Hupp, J. T.; Weaver, M. J. *J. Phys. Chem.* **1984**, *88*, 6128.

(29) The forms of eq 9a and 9b are obtained on the basis of simple geometrical considerations from a pair of intersecting parabolas with differing shapes (Figure 1). For the special case when these shapes are identical (i.e., $\lambda_f = \lambda_r$), the dimensionless parameter X is equivalent to Marcus' $-m$ parameter.[9b] For a related treatment for proton-transfer processes, see: Kresge, A. J. *Chem. Soc. Rev.* **1973**, *2*, 475.

(30) We are grateful to Prof. R. A. Marcus for clarifying this point to us.

(31) Cannon, R. D. *Chem. Phys. Lett.* **1977**, *49*, 277. Also see: German, E. D.; Kuznetsov, A. M. *Electrochim. Acta* **1981**, *26*, 1595.

(32) (a) Friedman, H. L.; Newton, M. D. *Discuss. Faraday Soc.* **1982**, *74*, 73. (b) Calef, D. F.; Wolynes, P. G. *J. Phys. Chem.* **1983**, *87*, 3387. (c) Ovchinnikova, M. Ya. *Russ. Theor. Exp. Chem.* **1981**, *17*, 507. (d) Weaver, M. J.; Gennett, T. *Chem. Phys. Lett.* **1985**, *113*, 213. (e) Gennett, T.; Milner, D.; Weaver, M. J. *J. Phys. Chem.*, this issue.

(33) Scher, T.; Holstein, T. *Philos. Mag.* **1981**, *B44*, 343.

(34) Although there is some ambiguity, the thermodynamic quantity $\Delta H'$ in eq 13 should apparently be an internal energy or enthalpy, rather than a free energy.[17,18] Since eq 13 is concerned only with the inner-shell mode, $\Delta H'$ should be an inner-shell portion of the overall thermodynamic reaction enthalpy, $\Delta H°$; thus $\Delta H'$ was roughly estimated from $\Delta H' = \Delta H°\lambda_{is}/(\lambda_{is} + \lambda_{os})$. Fortunately, the extent of the nuclear tunneling corrections was sufficiently small that these difficulties correspond to relatively small, ca. 2–3-fold or less, uncertainties in Γ_n and hence k_{calcd}.

(35) Thus, if the dependence of κ_{el} upon donor–acceptor separation distances, r, is $\kappa_{el} = \kappa_{el}° \exp[-\alpha(r - \delta)]$, where $\kappa_{el}°$ is the value of κ_{el} at the distance of closest approach, δ, then for the "typical" value of α, 1.5 Å^{-1},[36] the effective reaction zone thickness (the area under the $\kappa_{el} - r$ curve) is about 0.6 Å if $\kappa_{el}° = 1$.

TABLE I: Thermodynamic and Structural Parameters for Redox Couples in Aqueous Solution

redox couple[a]	E_f,[b] mV vs. SCE	$\Delta S°_{rc}$,[c] J K^{-1} mol^{-1}	a,[d] Å	Δa,[e] Å	ν_3,[f] cm^{-1}	ν_2,[g] cm^{-1}	$f_3 \times 10^{-5}$,[h] dyn cm^{-1}	$f_2 \times 10^{-5}$,[i] dyn cm^{-1}	ν_{is},[j] cm^{-1}
$Ru(OH_2)_6^{3+/2+}$	−16 (0.3)	151	3.25	0.09 ± 0.02[r]	532[w]	424[w]	2.98	1.90	434
$V(OH_2)_6^{3+/2+}$	−475 (0.2)	155	3.25	0.14 ± 0.02[s]	525[x]	380[bb]	2.92	1.52	435
$Fe(OH_2)_6^{3+/2+}$	500 (0.2)	180	3.25	0.13 ± 0.01	523[x]	379[cc]	2.90	1.52	434
$Cr(OH_2)_6^{3+/2+}$	−660 (1)	205	3.25	0.20 ± 0.03[t]	540[x]	380[bb]	3.09	1.52	439
$Co(OH_2)_6^{3+/2+}$	1680 (3)[k]	~250[p]	3.25	0.21 ± 0.02	548[x]	380[bb]	3.18	1.52	441
$Ru(NH_3)_6^{3+/2+}$	−183 (0.25)	75	3.35	0.04 ± 0.01	500[y]	460[y]	2.65	2.24	479
$Ru(en)_3^{3+/2+}$	−60 (0.1)	54	4.2	0.02 ± 0.02	~500[z]	~460[z]	2.65	2.24	479
$Co(en)_3^{3+/2+}$	−460 (1)	155	4.2	0.21 ± 0.02	485[y]	~357[dd]	2.44[dd]	1.28[dd]	407
$Ru(bpy)_3^{3+/2+}$	1040 (0.1)[l]	4	7.8	0[u]					
$Ru(phen)_2^{3+/2+}$	1041 (0.1)[m]	~4[q]	7.8	0[u]					
$Ru(terpy)_2^{3+/2+}$	1010 (0.1)[m]	~4[q]	7.8	0[u]					
$Fe(bpy)_3^{3+/2+}$	845 (0.05)	8	7.8	0[u]					
$Fe(phen)_3^{3+/2+}$	870 (0.05)	12	7.8	0.0 ± 0.01					
$Os(bpy)_3^{3+/2+}$	595 (0.5)[n]	~4[q]	7.8	0[u]					
	583 (0.1)[n]								
$Cr(bpy)_3^{3+/2+}$	−480 (0.1)[o]	16	7.8	0[u]					
$Co(bpy)_3^{3+/2+}$	70 (0.05)	92	7.8	0.19 ± 0.02[v]	~378[aa]	~243[aa]	2.44[dd]	1.28[dd]	289
$Co(phen)_3^{3+/2+}$	145 (0.05)	92	7.8	0.19 ± 0.02	378[aa]	243[aa]	2.44[dd]	1.28[dd]	289

[a] en = ethylenediamine, bpy = 2,2′-bipyridine, phen = 1,10-phenanthroline, terpy = 2,2′,2″-terpyridine. [b] Formal potential of redox couple vs. saturated calomel electrode at 25 °C (add 245 mV to convert to NHE). Ionic strength is given in parentheses. Data are from ref 39, except as noted. [c] Reaction entropy of redox couple. Data are from ref 39, except as noted. [d] Reactant radius. Estimates are from ref 14. [e] Change in metal–ligand bond length accompanying change of oxidation state. Taken from ref 14 except where noted. [f] Frequency of symmetrical metal–ligand bond vibration in M(III) state. [g] Frequency of symmetrical metal–ligand bond vibration in M(II) state. [h] Force constant for symmetrical metal–ligand bond vibration in M(III) state. Calculated by using eq 18, except as noted. [i] Force constant for symmetrical metal–ligand bond vibration in M(II) state. Calculated by using eq 18, except as noted. [j] Reduced frequency for metal–ligand bond vibration. Calculated according to $\nu_{is}^2 = 2\nu_3^2\nu_2^2/(\nu_3^2 + \nu_2^2)$. [k] Reference 57. [l] Reference 12. [m] Estimated for 0.1 M ionic strength from data in ref 12 and 58. [n] Reference 59. [o] Reference 60. [p] Estimated from thermodynamic data given in ref 61 by correcting for temperature dependence of reference electrode and likely ionic strength effects. [q] Assumed to equal $\Delta S°_{rc}$ for $Ru(bpy)_3^{3+/2+}$. [r] Reference 62. [s] Estimated as outlined in footnote 41. [t] Value is a weighted average of the axial and equatorial bond length changes (ref 14). [u] Assumed to equal Δd value for $Fe(phen)_3^{3+/2+}$. [v] Assumed to equal Δd value for $Co(phen)_3^{3+/2+}$. [w] Reference 15c. [x] Reference 15a. [y] From bulk-phase and surface-enhanced Raman data gathered in this laboratory. See ref 63. [z] Assumed to equal values for $Ru(NH_3)_6^{3+/2+}$. [aa] Reference 64. [bb] Assumed to equal value for $Fe(OH_2)_6^{2+}$. [cc] Reference 15b. [dd] Assumed to equal corresponding value for $Co(NH_3)_6^{3+/2+}$ (ref 16b).

expected if the reaction is nonadiabatic or is adiabatic only at the point of closest approach,[36] as given by the value of κ_{el} appearing in eq 5. (In the former case, $\kappa_{el} \ll 1$, and in the latter, $\kappa_{el} \sim 1$.)

Equations 2–13 along with the experimental parameters ϵ_{op}, ϵ_s, Δa, ν_{is}, $\Delta H°$, and $\Delta G°$ enable calculated values of k_{cor}, k_{calcd}, to be obtained for comparison with the measured rate constants.

(II) Activation Parameters. In addition to the rate constants at a single temperature, experimental activation parameters are also compared here with the corresponding theoretical predictions. We can write eq 2b and 5 as

$$k_{cor} = K_o\nu_n\Gamma_n\kappa_{el}\exp(\Delta S^*/R)\exp(-\Delta H^*/RT) \quad (14)$$

Calculated values of the activation entropy, ΔS^*_{calcd}, can be obtained for electrochemical reactions simply from[37]

$$\Delta S^*_{calcd} = \alpha_{calcd}\Delta S°_{rc} \quad (15)$$

where $\Delta S°_{rc}$ is the observed entropic driving force (i.e., the "reaction entropy")[39] and α_{calcd} is the calculated transfer coefficient, obtained from $\alpha_{calcd} = -(RT/F)(\mathrm{d}\ln k_{calcd}/\mathrm{d}E)$. Calculated activation entropies for homogeneous reactions are obtained from the equivalent expression[28] (see ref 28 for details)

$$\Delta S^*_{calcd} = \lambda_f X\Delta S°[\lambda_r^2 + (\lambda_f - \lambda_r)(\Delta G° + \lambda_r)]^{-1/2} \quad (16)$$

where $\Delta S°$ is the entropic driving force and X, λ_f, and λ_r have been defined above. Both eq 15 and 16 assume that the intrinsic activation entropy equals zero; this has been shown to be small (usually <10 J K^{-1}) even in the presence of specific reactant–solvent interactions.[40] Combined with the corresponding values of ΔG^*, ΔG^*_{calcd}, calculated as indicated above, these also enable corresponding calculated activation enthalpies to be evaluated from

$$\Delta H^*_{calcd} = \Delta G^*_{calcd} + T\Delta S^*_{calcd} \quad (17)$$

Since Γ_n is temperature dependent (eq 13), enthalpic and entropic nuclear-tunneling corrections, $\Delta S^*(Q)$ and $\Delta H^*(Q)$, respectively, can be added to both ΔH^*_{calcd} and ΔS^*_{calcd}, yielding the "semiclassical" quantities $\Delta H^*(T)$ and $\Delta S^*(T)$. These quantities are compared directly with the experimental work-corrected activation parameters, ΔH^*_{cor} and ΔS^*_{cor}, obtained from Arrhenius plots of $-R\ln k_{cor}$ vs. $(1/T)$ as outlined below.

Numerical Results

Table I summarizes the relevant thermodynamic, structural, and vibrational parameters for the various redox couples considered here that are utilized in the present calculations. The formal potentials, E_f, and reaction entropies, $\Delta S°_{rc}$, (both evaluated at ionic strengths around 0.1 M) enable the thermodynamic driving force terms $\Delta G°$, $\Delta H°$, and $\Delta S°$ to be evaluated. Thus for homogeneous reactions, $\Delta G° = F(E_{f,Ox} - E_{f,Red})$ and $\Delta S° = (\Delta S°_{rc,Red} - \Delta S°_{rc,Ox})$, where the subscripts Ox and Red refer to the redox couples undergoing oxidation and reduction, respectively, in the forward reaction. For the electrochemical reactions, $\Delta G° = F(E - E_f)$, where E is the applied electrode potential and $\Delta S°$ is given directly by the reaction entropy $\Delta S°_{rc}$. The effective reactant radii, a, and bond length differences, Δa, in Table I were largely taken from ref 14.[41] The stretching frequencies of the metal–ligand bonds in the oxidized and reduced states, ν_{Ox} and ν_{Red}, respectively, were obtained (or estimated) from Raman spectral data since the totally symmetrical (A_{1g}) mode provides

(36) (a) Newton, M. D. *ACS Symp. Ser.* **1982**, *No. 198*, 255. (b) Logan, J.; Newton, M. D. *J. Chem. Phys.* **1983**, *78*, 4086.

(37) The electrochemical activation entropy in eq 15, along with the corresponding activation enthalpies in eq 17, are the so-called "ideal" activation parameters; these are identified with the actual entropic and enthalpic barriers at the particular electrode potential to which they refer.[38]

(38) (a) Weaver, M. J. *J. Phys. Chem.* **1976**, *80*, 2645. (b) Weaver, M. J. *Ibid.* **1979**, *83*, 1748.

(39) Yee, E. L.; Cave, R. J.; Guyer, K. L.; Tyma, P. D.; Weaver, M. J. *J. Am. Chem. Soc.* **1979**, *101*, 1131.

(40) Hupp, J. T.; Weaver, M. J. *J. Phys. Chem.* **1984**, *88*, 1860.

(41) Since structural data are lacking for $V(OH_2)_6^{2+}$, the listed value of Δa for $V(OH_2)_6^{3+/2+}$ (0.14 Å) was estimated from the corresponding change in the oxide-based ionic radii for $V^{3+/2+}$ in relation to that for $Fe^{3+/2+}$, given the value of Δa for $Fe(OH_2)_6^{3+/2+}$ (0.13 Å). This procedure is supported by the close correspondence (within 0.01–0.02 Å) between metal–oxygen bond distances in oxides and in aquo complexes.

(42) Beattie, J. K.; Best, S. P.; Skelton, B. W.; White, A. H. *J. Chem. Soc., Dalton Trans.* **1981**, 2105.

TABLE II: Observed, Work-Corrected, and Calculated Rate Constants (M^{-1} s^{-1}) for Homogeneous Electron-Transfer Reactions at 25 °C

reaction	oxidant	reductant	k_{obsd}[a]	k_{cor}[b]	k_{calcd}[c]	ref
1	$V(OH_2)_6^{3+}$	$V(OH_2)_6^{3+}$	1.5×10^{-2} (2)	8×10^{-2}	8	65
2	$Fe(OH_2)_6^{3+}$	$Fe(OH_2)_6^{2+}$	4 (0.55)	52	60	66
3	$Co(OH_2)_6^{3+}$	$Co(OH_2)_6^{2+}$	8 (3)	33	4×10^{-8}	67
4	$Co(OH_2)_6^{3+}$	$Fe(OH_2)_6^{2+}$	50 (1)	4.2×10^{2}	8×10^{5}	68
5	$Co(OH_2)_6^{3+}$	$Cr(OH_2)_6^{2+}$	1.3×10^{4} (3)	5.3×10^{4}	4×10^{7}	69
6	$Co(OH_2)_6^{3+}$	$V(OH_2)_6^{2+}$	9×10^{5} (3)	3.7×10^{6}	1×10^{10}	69
7	$Fe(OH_2)_6^{3+}$	$Ru(OH_2)_6^{2+}$	2.3×10^{3} (1)	1.9×10^{4}	6×10^{6}	70
8	$Fe(OH_2)_6^{3+}$	$Cr(OH_2)_6^{2+}$	2.3×10^{3} (1)	1.9×10^{4}	2×10^{5}	71
9	$Fe(OH_2)_6^{3+}$	$V(OH_2)_6^{2+}$	1.8×10^{4} (1)	1.5×10^{5}	6×10^{7}	72
10	$Ru(OH_2)_6^{3+}$	$V(OH_2)_6^{2+}$	2.8×10^{2} (1)	2.3×10^{3}	6×10^{5}	70
11	$Fe(OH_2)_6^{3+}$	$Ru(NH_3)_6^{2+}$	3.5×10^{5} (0.1)	1.5×10^{7}	1.2×10^{9}	73
12	$Fe(OH_2)_6^{3+}$	$Ru(en)_3^{2+}$	1.4×10^{5} (0.1)	3.6×10^{6}	3×10^{9}	73
13	$Ru(OH_2)_6^{3+}$	$Ru(NH_3)_6^{2+}$	1.4×10^{4} (1)	1.1×10^{5}	5×10^{7}	70
14	$Ru(NH_3)_6^{3+}$	$Cr(OH_2)_6^{2+}$	2×10^{2} (0.2)	5.6×10^{3}	3×10^{3}	74
15	$Co(en)_3^{3+}$	$Cr(OH_2)_6^{2+}$	3×10^{-4} (1.0)	1.6×10^{-3}	1.5×10^{-3}	75
16	$Ru(NH_3)_6^{3+}$	$V(OH_2)_6^{2+}$	1.5×10^{3} (0.1)	6.5×10^{4}	7×10^{5}	76
17	$Co(en)_3^{3+}$	$V(OH_2)_6^{2+}$	4.6×10^{-4} (0.1)	1.2×10^{-2}	0.2	75
18	$Co(OH_2)_6^{3+}$	$Fe(phen)_3^{2+}$	1.4×10^{4} (3)	3.8×10^{4}	2.5×10^{9}	77
19	$Ru(bpy)_3^{3+}$	$Fe(OH_2)_6^{3+}$	6.4×10^{5} (1)	1.7×10^{6}	1.7×10^{10}	78
20	$Ru(phen)_3^{3+}$	$Fe(OH_2)_6^{2+}$	8×10^{5} (1)	2.2×10^{6}	1.7×10^{10}	78
21	$Ru(terpy)_3^{3+}$	$Fe(OH_2)_6^{2+}$	7.2×10^{5} (1)	2×10^{6}	1.7×10^{10}	78
22	$Fe(phen)_6^{2+}$	$Fe(OH_2)_6^{2+}$	3.7×10^{4} (0.5)	7.4×10^{4}	8×10^{8}	79
23	$Fe(bpy)_3^{3+}$	$Fe(OH_2)_6^{2+}$	2.7×10^{4} (0.5)	9.6×10^{4}	1.8×10^{9}	79
24	$Os(bpy)_3^{3+}$	$Fe(OH_2)_6^{2+}$	1.4×10^{3} (0.5)	5×10^{3}	6×10^{7}	80
25	$Fe(OH_2)_6^{3+}$	$Co(phen)_3^{2+}$	5.3×10^{3} (1)	1.4×10^{4}	6×10^{4}	75
26	$Co(phen)_3^{3+}$	$Cr(OH_2)_6^{2+}$	30 (1)	81	1.2×10^{3}	75
27	$Ru(bpy)_3^{3+}$	$Ru(OH_2)_6^{2+}$	1.9×10^{9} (1)	5.1×10^{9}	8×10^{12}	81
28	$Os(bpy)_3^{3+}$	$Ru(OH_2)_6^{2+}$	2.9×10^{8} (1)	7.8×10^{8}	4×10^{11}	70
29	$Co(phen)_3^{3+}$	$Ru(OH_2)_6^{2+}$	53 (1)	1.4×10^{2}	4×10^{4}	70
30	$Cr(bpy)_3^{3+}$	$V(OH_2)_6^{2+}$	4.2×10^{2} (1)	1.1×10^{3}	5×10^{6}	11
31	$Co(phen)_3^{3+}$	$V(OH_2)_6^{2+}$	4×10^{3} (1)	1.1×10^{4}	5×10^{5}	11
32	$Co(bpy)_3^{3+}$	$V(OH_2)_6^{2+}$	1.1×10^{3} (2)	2.3×10^{3}	1.6×10^{5}	82
33	$Ru(NH_3)_6^{3+}$	$Ru(NH_3)_6^{2+}$	4.3×10^{3} (0.1)	1.9×10^{5}	2×10^{6}	73
34	$Ru(en)_3^{3+}$	$Ru(NH_3)_6^{2+}$	2.7×10^{4} (0.1)	7.1×10^{5}	1.6×10^{8}	20a
35	$Ru(en)_3^{3+}$	$Ru(en)_3^{2+}$	2.8×10^{4} (0.75)	1.3×10^{5}	2.5×10^{7}	83
36	$Co(en)_3^{3+}$	$Co(en)_3^{2+}$	8×10^{-5} (1)	3×10^{-4}	2×10^{-4}	84
37	$Ru(bpy)_3^{3+}$	$Ru(phen)_3^{2+}$	4.2×10^{8} (0.1)	1.6×10^{9}	7×10^{8}	81
38	$Ru(bpy)_3^{3+}$	$Fe(phen)_3^{2+}$	1.8×10^{9} (1)	3.2×10^{9}	3×10^{10}	81
39	$Ru(bpy)_3^{3+}$	$Co(bpy)_3^{2+}$	2.4×10^{8} (1)	4.3×10^{8}	1.7×10^{10}	85
40	$Ru(bpy)_3^{3+}$	$Co(phen)_3^{2+}$	1.4×10^{8} (1)	2.5×10^{8}	9×10^{9}	85
41	$Co(phen)_3^{3+}$	$Co(phen)_3^{2+}$	40 (0.1)	1.5×10^{2}	2.5	86
42	$Co(bpy)_3^{3+}$	$Co(bpy)_3^{2+}$	20 (0.1)	74	2.5	86
43	$Co(bpy)_3^{3+}$	$Ru(NH_3)_6^{2+}$	1.1×10^{4} (0.1)	9.2×10^{4}	5×10^{6}	11
44	$Co(phen)_3^{3+}$	$Ru(NH_3)_6^{2+}$	1.5×10^{4} (0.1)	1.2×10^{5}	1.8×10^{7}	11
45	$Co(en)_3^{3+}$	$Cr(bpy)_3^{2+}$	35 (0.1)	2.2×10^{2}	7×10^{3}	87

[a] Observed rate constant for reaction between oxidant and reductant at ionic strengths noted in parentheses, from literature source noted in far right column. [b] Work-corrected rate constant; obtained from k_{obsd} by using eq 19. [c] Calculated rate constant, extracted from structural, vibrational, and formal potential data in Table I by using procedure detailed in the text.

the appropriate description of the reaction coordinate. (See footnotes to Table I for details and data sources.) The corresponding force constants, f_{Ox} and f_{Red}, were determined from

$$f_i = 4\pi^2 c^2 \mu \nu_i^2 \qquad (18)$$

where c is the velocity of light and μ is the reduced mass of the vibrating ligand. For the monodentate aquo and ammine ligands, μ was taken as the ligand mass. For cobalt couples containing large bidentate nitrogen-donor ligands, force constants were taken as equal to those for hexaamminecobalt since the appropriate reduced masses are uncertain.

Table II contains work-corrected rate constants, k_{cor}, for 45 homogeneous cross and self-exchange reactions involving these redox couples at 25 °C. These were obtained from the listed literature values of k_{obsd} by using[19a]

$$\log k_{cor} = \log k_{ob} + Z_A Z_B e^2 N / 2.303 RT\epsilon_s r(1 + \beta r \mu^{1/2}) \qquad (19)$$

where Z_A and Z_B are the charge numbers of the two reactants, r is the sum of the reactant radii (Table I), β is the Debye–Huckel parameter, and μ is the ionic strength (listed in parenthesis in Table II along with the literature sources). Listed alongside these values of k_{cor} are the corresponding calculated values, k_{calcd}, obtained from the parameters in Table I by using eq 2–13. (Relevant parameters obtained in these calculations, λ_f, λ_r, Γ_n, $\Delta G^*(T)$, K_o, and Γ_n, are listed in Table S-1, supplementary material.)

TABLE III: Comparison of Solvent Reorganization Energies, λ_{os}, Calculated from Eq 11a and 11b for Selected Reaction Types in Aqueous Solution

reaction	λ_{os}, kJ mol^{-1}		
	eq 11a[a]	eq 11b[b]	eq 11b[c]
$M(OH_2)_6^{3+} + M(OH_2)_6^{2+}$	116	167	115
$M(en)_3^{3+} + M(en)_3^{2+}$	90	129	97
$M(bpy)_3^{3+} + M(bpy)_3^{2+}$	55	80	67
$M(OH_2)_6^{3+} + M(bpy)_3^{2+}$	96	82	65

[a] Determined with $a_1 + a_2 = R_h$, i.e., for reactants in contact, with reactant radii taken from Table I. [b] Determined for ellipsoid formed with spherical reactants in contact, based on radii in Table I. [c] Determined for ellipsoid formed with 1.25-Å interpenetration between spherical reactants.

The value of l_a in eq 11b was obtained by taking the internuclear separation, r, as 1.25 Å less than the sum of the radii ($a_1 + a_2$). This choice is based on the likelihood that such ligand interpenetration will occur as a result of reaction nonadiabaticity.[18,36] The value of l_b was calculated by taking the ellipsoid volume to equal that of the two isolated reactant spheres. For most systems, the values of λ_{os} obtained on this basis are not greatly different from those obtained from eq 11a with the reactant spheres as-

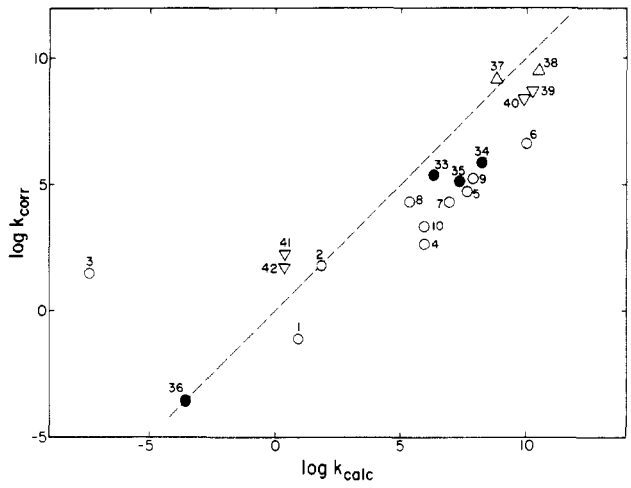

Figure 2. Logarithm of the electrostatic work-corrected rate constants for homogeneous reactions between complexes having identical ligand compositions plotted against the logarithm of the corresponding calculated rate constants. Data from Table II: (○) aquo complexes, (●) ammine and ethylenediamines; (△) polypyridines. Reaction identification numbers are those listed in Table II.

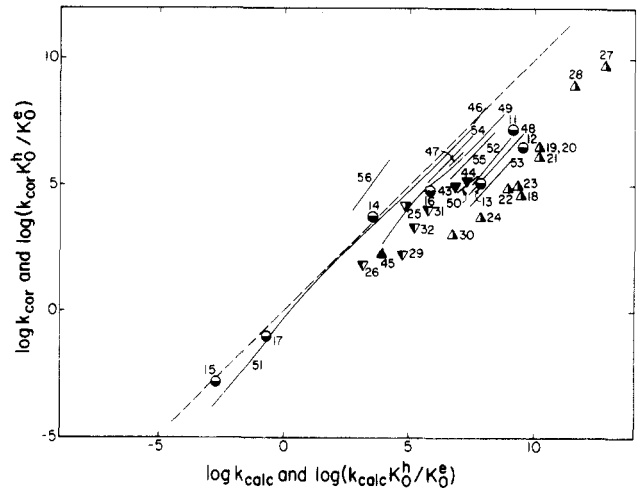

Figure 3. Logarithm of the electrostatic work-corrected rate constants for electrochemical reactions and homogeneous cross reactions between complexes with dissimilar ligand compositions plotted against the logarithm of the corresponding calculated rate constants. Data from Tables II and IV. Electrochemical rate constants are converted to "equivalent second-order" rate constants by using eq 20: (⊖) aquo–ammine; (△) aquo–low spin polypyridine; (▽) aquo–Co(III)/(II) polypyridine; (▲) ammine–low spin polypyridine; (▼) ammine–Co(III)/(II) polypyridine. Electrochemical rate–driving force data shown as solid lines. Reaction identification numbers are those listed in Tables II and IV.

sumed to be in contact (i.e., $a_1 + a_2 = R_h$). As an illustration, values of λ_o are given in Table III for four reaction types obtained from eq 11b (assuming 1.25 Å interpretation), and from eq 11a and 11b (assuming reactant contact). (Note that a 10 kJ mol^{-1} variation in λ_o corresponds to only a ca. 2.5-fold difference in k_{cor}.)

A corresponding set of experimental electrochemical rate constants, k_{cor}^e, for the reduction of several aquo and ammine complexes at the mercury–aqueous interface are summarized in Table IV. These are obtained from rate–potential data gathered in our laboratory by applying electrostatic double-layer corrections; (see the relevant papers for details[2,3,8,43,44]). Where available, values of k_{cor} are given at several representative driving forces (i.e., overpotentials), denoted by the $\Delta G°$ values in Table IV. Values of k_{cor} for one reaction, $Cr(OH_2)_6^{3+}$ reduction, are also given at several other electrodes, namely gallium, lead, and underpotential deposited (upd) lead/silver and thallium/silver surfaces. These and data for related reactions were obtained in order to examine quantitatively the influence of the metal substrate upon the kinetics of such outer-sphere reactions.[45] (Note that values of k_{cor} are given for reduction of the tripositive complexes at anodic as well as cathodic overpotentials; i.e., for positive as well as negative values of $\Delta G°$.)

In order to compare the electrochemical and the homogeneous rate data with the theoretical predictions on a common basis, the former rate constants are also listed in Table IV in the form of equivalent second-order rate constants, k_{cor}' (M^{-1} s^{-1}) obtained from k_{cor}^e by using

$$k_{cor}' = k_{cor}^e K_o^h / K_o^e \qquad (20)$$

where K_o^h and K_o^e are obtained from eq 3 and 4 with $\delta r_e = \delta r_h$ and r_h set equal to twice the reactant radius. (These values of k_{cor}' refer to the hypothetical reaction of the complex at the metal surface if the latter formed a coreacting sphere of equal radius to that of the reactant.) The corresponding calculated values, k_{calcd}', also given in Table IV, were obtained as outlined above, with R_e (eq 10) taken as 14 Å,[2] and also converted to effective second-order values by means of eq 20.

The corresponding values of k_{cor} and k_{calcd} for the homogeneous reactions in Table II are also presented as plots of log k_{cor} against log k_{calcd} in Figures 2 and 3. The former plot contains reactions between complexes having identical ligand compositions and the latter between those having unlike coordination shells. Figure 3 also contains effective second-order electrochemical rate constants (Table IV); these can be considered to refer to "cross reactions" where the metal surface replaces the coreacting solution species. The electrochemical entries are shown as solid curves in Figure 3, reflecting the range of driving force over which the electrochemical rate data are obtained.

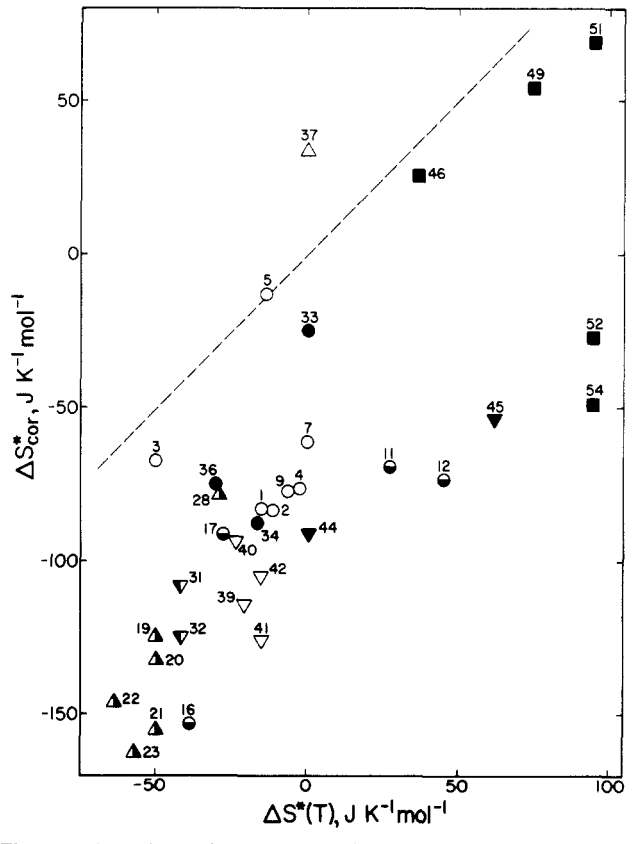

Figure 4. Experimental work-corrected activation entropies for homogeneous and electrochemical reactions plotted against corresponding calculated parameters. Data from Tables S-2 and S-3. Key to reaction types: (■) electrochemical; others as in Figures 2 and 3. Reaction identification numbers listed in Tables II and IV.

Figure 4 is a plot of the "experimental" work-corrected activation entropies, ΔS^*_{cor}, vs. the corresponding calculated activation

(43) Tyma, P. D.; Weaver, M. J. *J. Electroanal. Chem.* **1980**, *111*, 195.
(44) Gennett, T.; Weaver, M. J. *Anal. Chem.* **1984**, *56*, 1444.
(45) Liu, H. Y.; Hupp, J. T.; Weaver, M. J. *J. Electroanal. Chem.* **1984**, *179*, 219.

TABLE IV: Experimental and Calculated Rate Constants for Electrochemical Reduction Reactions at 25 °C

no.	reaction	$\Delta G°$,[a] kJ mol^{-1}	k_{cor},[b] cm s^{-1}	k_{cor}',[c] M^{-1} s^{-1}	k_{calcd}',[d] M^{-1} s^{-1}	ref
46	$Ru(NH_3)_6^{3+}$ at mercury	0	2.5	5.6×10^7	5.6×10^7	8, 44
47	$Ru(OH_2)_6^{3+}$ at mercury	0	5×10^{-2}	1×10^6	4.5×10^6	2
48	$Fe(OH_2)_6^{3+}$ at mercury	−20	2.6×10^{-3}	5.5×10^4	2×10^7	43, 88
		−30	1.6×10^{-2}	3.4×10^5	1.3×10^8	
		−40	9×10^{-2}	2×10^6	7×10^8	
		−50	6×10^{-1}	1.3×10^7	3×10^9	
49	$V(OH_2)_6^{3+}$ at mercury	30	4×10^{-7}	7	1.1×10^2	2
		20	9×10^{-6}	1.8×10^2	1.3×10^3	
		10	1.2×10^{-4}	2.6×10^3	1.5×10^4	
		0	8×10^{-4}	1.6×10^4	1.4×10^5	
		−10	6×10^{-3}	1.3×10^5	1.2×10^6	
50	$V(OH_2)_6^{3+}$ at lead	−20	2.6×10^{-3}	5×10^4	9×10^6	45
		−30	1.1×10^{-2}	2×10^5	6×10^7	
		−40	4×10^{-2}	9×10^5	3×10^8	
51	$Cr(OH_2)_6^{3+}$ at mercury	90	5×10^{-8}	1×10^{-10}	4×10^{-9}	2, 37b
		80	1.6×10^{-16}	3×10^{-9}	7×10^{-8}	
		70	5×10^{-15}	9×10^{-8}	1.2×10^{-6}	
		60	1.3×10^{-13}	3×10^{-6}	2×10^{-5}	
		50	3×10^{-12}	7×10^{-5}	3×10^{-4}	
		40	8×10^{-11}	1.7×10^{-3}	5×10^{-3}	
		30	2×10^{-9}	4×10^{-2}	6×10^{-2}	
		20	4×10^{-8}	7×10^{-1}	8×10^{-1}	
		10	4×10^{-7}	8	9	
		0	3×10^{-6}	7×10^1	9×10^1	
		−10	3×10^{-5}	6×10^2	9×10^2	
		−20	2×10^{-4}	4×10^3	8×10^3	
		−30	1.6×10^{-3}	3×10^4	6×10^4	
		−40	1.2×10^{-2}	2.5×10^5	4×10^5	
		−50	9×10^{-2}	2×10^6	3×10^6	
52	$Cr(OH_2)_6^{3+}$ at lead	−40	6×10^{-4}	1.3×10^5	6×10^4	45
		−50	5×10^{-3}	1.1×10^5	4×10^5	
		−60	5×10^{-2}	1×10^6	1.7×10^7	
53	$Cr(OH_2)_6^{3+}$ at gallium	−50	8×10^{-4}	1.4×10^4	4×10^5	45
		−60	6×10^{-3}	1×10^5	1.7×10^7	
54	$Cr(OH_2)_6^{3+}$ at upd lead/silver	−20	8×10^{-4}	1.7×10^4	8×10^3	45
		−30	7×10^{-3}	1.4×10^5	6×10^4	
		−40	6×10^{-2}	1×10^6	4×10^5	
55	$Cr(OH_2)_6^{3+}$ at upd thallium/silver	−30	8×10^{-2}	1.6×10^6	6×10^4	45
		−40	1×10^{-2}	2×10^5	4×10^5	
		−50	1.4×10^{-3}	2.8×10^4	3×10^6	
56	$Co(en)_3^{3+}$ at mercury	0	2.5×10^{-2}	1×10^6	1.3×10^4	89

[a] Free-energy driving force, obtained from overpotential ($E - E_f$), using $\Delta G° = F(E - E_f)$. [b] Work-corrected electrochemical rate constant. From rate–overpotential data given in references indicated. [c] Work-corrected rate constant expressed in equivalent second-order units obtained from k_{cor} by using eq 20 (see text). [d] Calculated rate constant, expressed in equivalent second-order units by using eq 20 (see text).

entropies, $\Delta S^*(T)$, obtained as outlined above. The corresponding plot of the "electrostatic work-corrected" activation enthalpies, ΔH^*_{cor}, vs. the calculated activation enthalpies, $\Delta H^*(T)$, is given in Figure 5. For the homogeneous reactions, the ΔH^*_{cor} were extracted from the observed activation enthalpies (obtained from the slope of the Arrhenius plot of $-R \ln k_{obsd}$ vs. $(1/T)$[46]) by assuming that the work correction embodied in eq 19 is wholly contained in the enthalpic component. The rationale for this presumption derives from the observation that the enthalpy, but not the entropy, of activation for outer-sphere reactions depends upon the ionic strength.[20a,47] For the electrochemical reactions, values of ΔH^*_{cor} were obtained from the temperature dependence of k_{cor} at a fixed electrode potential by using a nonisothermal cell arrangement. (These are so-called "ideal" parameters; see ref 37b and 45 for details.) The values of ΔS^*_{cor} were determined from ΔH^*_{cor} by inserting this into eq 14 along with k_{cor}, K_o, and ν_n and setting κ_{el} equal to unity. (The nuclear tunneling term is thereby contained in the experimental activation parameters themselves.)

Complete listings of ΔS^*_{cor}, $\Delta S^*(T)$, $\Delta S°$, ΔH^*_{cor}, $\Delta H^*(T)$, and $\Delta H°$ are given in Tables S-2 and S-3, respectively (supplementary material).

Discussion

Inspection of the rate data in Tables II and IV and Figures 2 and 3 reveals that the values of k_{calcd} obtained from the theoretical approach embodied in eq 2–17 largely account for the enormous (ca. 10^{14}-fold) variations in the experimental rate constants, k_{cor}. Nevertheless, the latter values are almost uniformly smaller than the former for both homogeneous and electrochemical reactions by factors typically between 10 and 10^3. A qualitatively similar observation, albeit for a much more limited range of systems, was made by Sutin et al.[14] in their examination of rate constants for homogeneous self-exchange reactions obtained directly and inferred from cross-reaction data.

It is useful to scrutinize these findings as a function of reactant electronic structure, ligand composition, and the reaction thermodynamics. The greatest uncertainties in the calculated free-energy barriers, and hence in k_{calcd}, will clearly be for reactions having the largest inner-shell barriers and therefore the smallest values of k_{calcd}. However, the extent of the differences between log k_{cor} and log k_{calcd} does not exhibit any clear dependence on the magnitude of k_{calcd} (Figures 2, 3). A related matter concerns the possible dependence of the discrepancies between k_{cor} and k_{calcd} upon $\Delta G°$. Figure 6 is a plot of (log k_{calcd} − log k_{cor}) against the "reduced" driving force term $-2\Delta G°/(\lambda_f + \lambda_r)$. (The denominator normalizes $\Delta G°$ to the magnitude of the intrinsic barrier.) Al-

(46) It is conventional in the homogeneous redox literature to include in the observed Arrhenius activation enthalpy $\Delta H^‡$ the temperature dependence of the "Eyring" preexponential factor kT/h, since this term commonly appears in kinetic formulations. (These literature values are listed in Table S-2.) This correction is inappropriate on the basis of the encounter preequilibrium treatment employed here since the preexponential factor is anticipated to be temperature independent, so that the desired activation enthalpy ΔH^* is related to $\Delta H^‡$ by $\Delta H^* = \Delta H^‡ + RT$.

(47) Ekstrom, A.; McLaren, A. B.; Smythe, L. E. *Inorg. Chem.* **1976**, *15*, 2853.

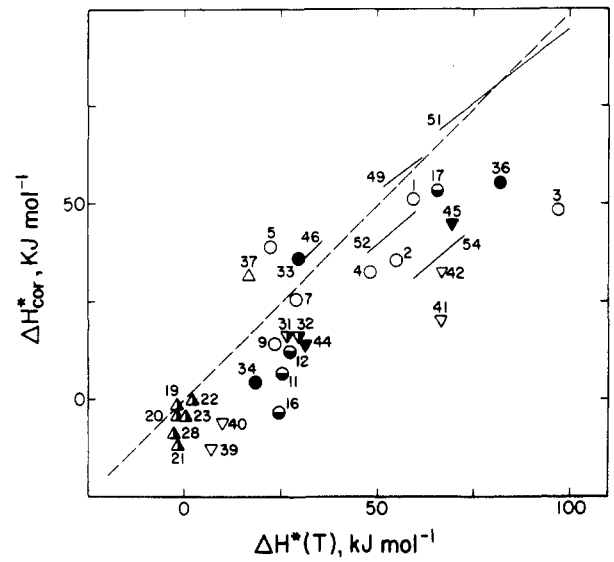

Figure 5. Experimental work-corrected activation enthalpies for homogeneous and electrochemical reactions plotted against corresponding calculated parameters. Data from Tables S-2 and S-3. Electrochemical data shown as solid lines, homogeneous data as points, with symbols as in Figures 2 and 3. Reaction identification numbers as in Tables II and IV.

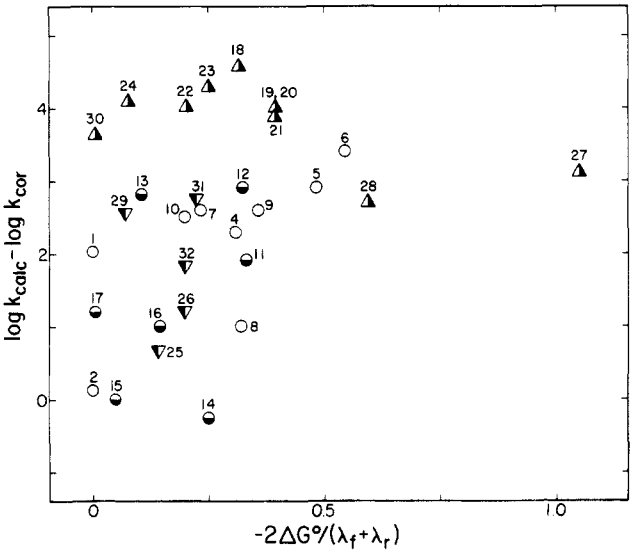

Figure 6. Logarithm of discrepancies between calculated and work-corrected rate constants for homogeneous reactions (log k_{calcd} − log k_{cor}) plotted against "reduced" free-energy driving force, $2\Delta G°/(\lambda_f + i_r)$. Reaction identification numbers as in Table II.

though the values of (log k_{calcd} − log k_{cor}) show considerable scatter, they do not exhibit any noticeable decrease with increasing driving force.

This persistence of such discrepancies between log k_{cor} and log k_{calcd} for reactions having small ΔG^* indicates that their origin is not associated primarily with systematic errors in calculating ΔG^*, since such errors in both the inner- and outer-shell components will necessarily diminish as ΔG^* decreases. In contrast, the composite preexponential factor, $K_o\nu_n\kappa_{el}$ (eq 2, 5), is not expected to be sensitive to the magnitude of ΔG^*, so that these terms are the likely sources of the disparities between k_{cor} and k_{calcd}.

Further insight into this question can in principle be gleaned by comparing the experimental and calculated activation parameters (Figures 4, 5). As noted above, a key assumption made in deriving the calculated rate parameters is that the reaction pathways are adiabatic at the point of closest approach of the coreacting centers, i.e., $\kappa_{el} = 1$ in eq 5 and 14. However, there is increasing evidence to suggest that $\kappa_{el} < 1$ even for reactions involving small inorganic complexes in both homogeneous[1c,18,36] and electrochemical[7,48-50] environments. Recent ab initio calculations for $Fe(OH_2)_6^{3+/2+}$ self-exchange indicate that $\kappa_{el} \sim 0.1$ even for a transition-state geometry involving interpenetration of the aquo ligands.[36] If such nonadiabaticity is primarily responsible for the observation that $k_{cor} < k_{calcd}$, one would expect that these discrepancies would be chiefly contained in the entropic component, i.e., that $R(\ln k_{cor} - \ln k_{calcd}) \approx \Delta S^*_{cor} - \Delta S^*(T)$, since it was assumed that $\kappa_{el} = 1$ when extracting ΔS^*_{cor} from the observed Arrhenius parameters. The occurrence of a subunity steric factor, anticipated as an additional consequence of reaction pathways featuring ligand interpenetration, will also yield smaller values of ΔS^*_{cor}. Inspection of Figure 4 reveals that indeed $\Delta S^*_{cor} < \Delta S^*(T)$ for most reactions. However, the typical differences $\Delta S^*_{cor} - \Delta S^*(T)$, ca. −60 to −90 J K^{-1} mol^{-1}, are equivalent to 10^3–10^5-fold disparities between k_{cor} and k_{calcd}, rather larger than are actually observed. This is because typically $\Delta H^*_{cor} < \Delta H^*(T)$ (Figure 5), i.e., partial enthalpic–entropic compensation is encountered

This suggests that at least part of the discrepancies between k_{cor} and k_{calcd} are associated instead with changes in reactant–solvent interactions necessitated by the approach of the two reactants (or the reactant to the metal surface). Such an effect would yield a work term component additional to that described by the Debye–Huckel and Gouy–Chapman models used here, consisting of partially compensating negative enthalpic and entropic components.[12] Although distinct, the nonadiabatic and solvent work term effects may nonetheless be closely coupled since the occurrence of nonadiabatic pathways will constrain the reaction to occur chiefly via transition states with the electron donor and acceptor sites in very close proximity. Especially since suitable geometrical configurations may necessitate interpenetration of the ligand envelopes,[18] the changes in reactant–solvent interactions required to form the precursor state could be substantial. Tembe et al. have shown that suitably negative, and moreover ionic strength independent, values of ΔS^*_{cor} for $Fe(OH_2)_6^{3+/2+}$ self-exchange are obtained by using a theoretical model based on ion-pair correlation functions along with ligand interpenetration.[18] We have shown that intrinsic activation entropies should be only mildly influenced by the occurrence of specific reactant–solvent interactions after correction for work terms.[40]

The electrochemical reactions at mercury are of particular interest in this regard since mercury surfaces are known to have only a small affinity for water (i.e., are relatively "hydrophobic")[51] and therefore may perturb the structural environment, and hence the reaction energetics, of the reacting species to an unusually small extent. This is borne out by the observation that the corresponding values of k_{cor} and k_{calcd} for most reactions at mercury are not greatly different, the typically ca. 2–20-fold smaller values of k_{cor} relative to k_{calcd} (Table IV, Figure 3) being associated largely with the entropic component, i.e., $\Delta S^*_{cor} < \Delta S^*(T)$. Together with evidence obtained from a comparison of the kinetics of parallel inner- and outer-sphere pathways at mercury,[7] this suggests that the mercury surface provides a weakly interacting, marginally nonadibatic ($\kappa_{el} \sim 0.1$) reaction environment. The strikingly smaller rate constants, and especially activation parameters, obtained at lead, upd surfaces, and at gallium are particularly interesting since these surfaces are known to have a much greater tendency to bind water molecules (i.e., are more "hydrophilic") than mercury.[51] These data are discussed in detail elsewhere.[8,45] It suffices to note here that the magnitude as well as nature of the discrepancies [$k_{cor} < k_{calcd}$, $\Delta S^*_{cor} < \Delta S^*(T)$, $\Delta H^*_{cor} < \Delta H^*(T)$] seen for reactions at these hydrophilic surfaces are remarkably similar to those observed between pairs of cationic reactants in homogeneous solution (Figure 3). This suggests that these discrepancies may have a common origin, being associated

(48) Li, T. T.-T.; Liu, H. Y.; Weaver, M. J. *J. Am. Chem. Soc.* **1984**, *106*, 1233.
(49) Li, T. T.-T.; Guyer, K. L.; Barr, S. W.; Weaver, M. J. *J. Electroanal. Chem.* **1984**, *164*, 27.
(50) Li, T. T.-T.; Weaver, M. J. *J. Am. Chem. Soc.* **1984**, *106*, 6107.
(51) Trassati, S. "Modern Aspects of Electrochemistry"; Conway, B. E., Bockris, J. O'M., Eds.; Plenum: New York, 1979; Vol. 13, p 81. Trassati, S. *Electrochim. Acta* **1983**, *28*, 1083.

primarily with changes in local solvent structure in the vicinity of the reaction site.

One unexpected feature of the data in Figure 3 is the especially large (ca. 10^2–10^3) discrepancies between k_{cor} and k_{calcd} for reactions between aquo and low-spin polypyridine redox couples. One possibility is that the ellipsoid model (eq 11b) used to calculate k_{calcd} underestimates the outer-shell reorganization energy for these particular reactions. Indeed the use of eq 11a assuming reactant "contact" yields a substantially larger reorganization energy for aquo–polypyridine reactions than from eq 11b assuming ligand "interpenetration" (Table III); this corresponds to ca. 10-fold smaller estimates of k_{calcd} when the former is used. In any case, the employment of such simple outer-shell models for polypyridine reactants is rather doubtful given their nonspherical nature. Nevertheless, for reactions between pairs of polypyridine complexes, $k_{cor} \sim k_{calcd}$ (Figure 2).

A related source of deviations between k_{cor} and k_{calcd} lies in the underlying limitations of the dielectric continuum model in estimating the outer-shell barrier. We have recently analyzed in detail the sources and likely magnitude of additional "noncontinuum" contributions to the intrinsic barrier associated with specific ligand–solvent interactions.[52] Although often predicted to be small ($\lesssim$1 kcal mol^{-1}),[52] they are likely to contribute significantly to the smaller values of k_{cor} relative to k_{calcd}, especially for reactions involving aquo and ammine complexes that interact strongly with surrounding solvent molecules.

By and large, the discrepancies between the calculated and observed rate parameters do not show any clear-cut dependence on the metal electronic structure. Of particularly interest in this regard are reactions involving high-spin Co(III)/(II) couples since these have often been suspected to be especially nonadiabatic.[1d,53] In fact k_{cor} for reactions involving Co(III)/(II) polypyridine couples tend to be larger relative to k_{calcd} than that for those involving corresponding low-spin polypyridines (Figures 2, 3). This finding, which is opposite to that expected if $\kappa_{el} \ll 1$ for the Co(III)/(II) reactions, is likely to be due to systematic errors in calculating the especially large inner-shell barriers for Co(III)/(II). It is therefore advantageous to compare instead the observed and calculated activation entropies (Figure 4) since the latter are insensitive to errors in calculating the inner-shell barriers. Although the points are scattered, it is seen that the reactions involving high-spin Co(III)/(II) couples (points 31, 32, 36, 40, 41, 44, and 45, Figure 4) do not display any unusually large discrepancies between ΔS^*_{corr} and $\Delta S^*(T)$. This suggests that the Co(III)/(II) reactions are not substantially more nonadiabatic since unusually negative values of ΔS^*_{cor} should thereby result. (Note that a tenfold decrease in κ_{el} would be reflected in a 20 J K^{-1} mol^{-1} decrease in ΔS^*_{cor}.)

Although for most systems in Figures 2 and 3, $k_{cor} \lesssim k_{calcd}$, there are a few notable exceptions. The observation that $k_{cor} \gg k_{calcd}$ for $Co(OH_2)_6^{3+/2+}$ self-exchange (point 3, Figure 2) is probably due to the occurrence of an inner-sphere pathway.[54] For almost all other reactions between aquo complexes, k_{cor} is 10–100-fold smaller than k_{calcd}. The exception is $Fe(OH_2)_6^{3+/2+}$ self-exchange where $k_{cor} \approx k_{calcd}$; this reaction may also occur via an "abnormal", possibly water-bridged, pathway.[5] The finding that $k_{cor} > k_{calcd}$ for $Co(en)_3^{3+/2+}$ at mercury (Figure 3) is initially surprising given that $k_{cor} \lesssim k_{calcd}$ for $Co(en)_3^{3+/2+}$ in homogeneous reaction environments (points 17, 36, and 45, Figure 3). This almost certainly arises from weak adsorption of $Co(en)_3^{3+/2+}$, resulting from the hydrophobic nature of the ethylenediamine ligands.[8,55] Indeed, adsorption of polypyridine couples at mercury precludes accurate measurement of rate parameters for these hydrophobic systems. Unexpectedly rapid electrochemical reactivities are also obtained at the mercury–aqueous interface with reactants containing a variety of hydrophobic organic ligands.[56]

Concluding Remarks

In a global sense contemporary electron-transfer theory is moderately successful in predicting outer-sphere rate constants involving cationic redox couples in both homogeneous and heterogeneous aqueous environments. Nevertheless, the systematic deviations observed between the calculated and observed rate parameters clearly indicate the presence of significant additional factors that are not included in the theoretical treatment employed here. The smaller values of k_{cor} relative to k_{calcd} seem likely to be due predominantly to local solvent structural changes brought about by the approach of the reacting centers. Reaction nonadiabaticity may also contribute importantly by constraining the reactants to be in very close proximity in order to yield suitably large values of κ_{el}. Although other shortcomings of the theoretical calculations undoubtedly contribute, such as anharmonicity of the inner-shell barrier and noncontinuum components of the outer-shell barrier, the major origin of these discrepancies probably lies in errors in estimating the preexponential factor rather than in the energetics of the elementary electron-transfer step.

These results illustrate the important virtues of employing a unified data treatment for homogeneous and heterogeneous redox processes. This approach enables rate parameters for both types of redox process to be examined on a common basis, thereby directly exposing the similarities and differences of electrode surfaces and solution species as outer-sphere reagents.

(52) Hupp, J. T.; Weaver, M. J. *J. Phys. Chem.*, *1984*, *88*, 6128.
(53) Buhks, E.; Bixon, M.; Jortner, J.; Navon, G. *Inorg. Chem.* **1979**, *18*, 2014.
(54) Endicott, J. F.; Durham, B.; Kumar, K. *Inorg. Chem.* **1982**, *21*, 2437.
(55) Tadayyoni, M. A.; Weaver, M. J. *J. Electroanal. Chem.*, in press.
(56) Li, T. T.-T.; Weaver, M. J. *Inorg. Chem.*, in press.
(57) Huchital, D. N.; Sutin, N.; Warnquist, B. *Inorg. Chem.* **1967**, *6*, 838.
(58) Dwyer, F. P.; Gyarfas, E. C. *J. Am. Chem. Soc.* **1954**, *76*, 6320.
(59) Dwyer, F. P.; Gibson, N. A.; Gyarfas, E. C. *Proc. R. Soc. N.S.W.* **1950**, *84*, 80.
(60) Sahami, S.; Weaver, M. J. *J. Electroanal. Chem.* **1981**, *122*, 171.
(61) Noyes, A. A.; Deahl, T. J. *J. Am. Chem. Soc.* **1937**, *59*, 1337.
(62) Bernhard, P.; Burgi, H. B.; Hauser, J.; Lehmann, H.; Ludi, A. *Inorg. Chem.* **1982**, *21*, 3936.
(63) Tadayyoni, M. A.; Farquharson, S.; Weaver, M. J. *J. Chem. Phys.* **1984**, *80*, 1363.
(64) Saito, Y.; Takemoto, J.; Hutchinson, B.; Nakamoto, K. *Inorg. Chem.* **1972**, *11*, 2003.
(65) Krishnamurty, K. V.; Wahl, A. C. *J. Am. Chem. Soc.* **1958**, *80*, 5921.
(66) Silverman, J.; Dodson, R. W. *J. Phys. Chem.* **1952**, *56*, 846.
(67) Habib, H. S.; Hunt, J. P. *J. Am. Chem. Soc.* **1966**, *88*, 1668.
(68) Bennett, L. E.; Sheperd, J. L. *J. Phys. Chem.* **1962**, *66*, 1275.
(69) Hyde, M. R.; Davies, R.; Sykes, A. G. *J. Chem. Soc., Dalton Trans.* **1972**, 1838.
(70) Bottcher, W.; Brown, G. M.; Sutin, N. *Inorg. Chem.* **1979**, *18*, 1447.
(71) Dulz, G.; Sutin, N. *J. Am. Chem. Soc.* **1964**, *86*, 829.
(72) Ekstrom, A.; McLaren, A. B.; Smythe, L. E. *Inorg. Chem.* **1976**, *15*, 2853.
(73) Meyer, T. J.; Taube, H. *Inorg. Chem.* **1968**, *7*, 2369.
(74) Endicott, J. F.; Taube, H. *J. Am. Chem. Soc.* **1964**, *86*, 1686.
(75) Przystas, T. J.; Sutin, N. *J. Am. Chem. Soc.* **1973**, *95*, 5545.
(76) Jacks, C. A.; Bennett, L. E. *Inorg. Chem.* **1974**, *13*, 2035.
(77) Campion, R. J.; Purdie, N.; Sutin, N. *Inorg. Chem.* **1964**, *3*, 1091.
(78) Braddock, J. N.; Meyer, T. J. *J. Am. Chem. Soc.* **1973**, *95*, 3158.
(79) Ford-Smith, N. J.; Sutin, N. *J. Am. Chem. Soc.* **1961**, *83*, 1830.
(80) Gordon, B. M.; Williams, L. L.; Sutin, N. *J. Am. Chem. Soc.* **1961**, *83*, 2061.
(81) Young, R. C.; Keene, F. R.; Meyer, T. J. *J. Am. Chem. Soc.* **1977**, *99*, 2468.
(82) Davies, R.; Green, M.; Sykes, A. G. *J. Chem. Soc., Dalton Trans.* **1972**, 1171.
(83) Beattie, J. K., cited in ref 14.
(84) Dwyer, F. P.; Sargeson, A. M. *J. Phys. Chem.* **1961**, *65*, 1892.
(85) Berkoff, R.; Krist, K.; Gafney, H. D. *Inorg. Chem.* **1980**, *19*, 1.
(86) Neumann, H. M., quoted in: Farina, R.; Wilkins, R. G. *Inorg. Chem.* **1968**, *7*, 514.
(87) Beattie, J. K.; Binstead, R. A.; Broccardo, M. *Inorg. Chem.* **1978**, *17*, 1822.
(88) Weaver, M. J.; Tyma, P. D.; Nettles, S. M. *J. Electroanal. Chem.* **1980**, *114*, 53.
(89) Sahami, S.; Weaver, M. J. *J. Electroanal. Chem.* **1981**, *124*, 35.

Acknowledgment. We are indebted to Dr. J. K. Beattie (University of Sydney) for communicating some Raman spectroscopic data prior to publication. The manuscript benefited from some helpful suggestions by Prof. R. A. Marcus. This work is supported in part by the Air Force Office of Scientific Research and the Office of Naval Research. M.J.W. acknowledges a fellowship from the Alfred P. Sloan Foundation.

Supplementary Material Available: Tables of calculated electron-transfer parameters for homogeneous and electrochemical reactions, experimental and calculated activation parameters for homogeneous electron-transfer reactions, and experimental and calculated activation parameters for electrochemical electron-transfer reactions (8 pages). Ordering information is given on any current masthead page.

Damped Dispersion Energies of Some van der Waals Molecules

Marcy E. Rosenkrantz,*† Rebecca M. Regan, and Daniel D. Konowalow

Department of Chemistry, State University of New York, Binghamton, New York 13901
(Received: February 6, 1985)

The method of Krauss, Neumann, and Stevens (KNS) to obtain damped dispersion energies has been assessed by treating the lowest $^3\Sigma_u^+$ state of Li_2, the $^3\Sigma^+$ state of LiNa, the lowest $^3\Sigma_u^+$ state of Li_2^+, and the lowest $^2\Sigma^+$ state of NaAr. While the KNS method assumes that the exchange correlation energy, E_{xcorr}, is negligible, we find it to be substantial for Li_2. We correct the damped dispersion energy for LiNa with an estimated E_{xcorr} term to obtain a corrected potential curve which appears to be quite reliable.

I. Introduction

Krauss, Neumann, and Stevens (KNS) have introduced a method[1-4] to obtain damped dispersion interaction energies for closed- and open-shell atomic systems. Based on a method proposed by Koide,[5] it accounts for the modulation of the dispersion energy due to charge cloud overlap. It retains the physical appeal and the familiarity of a multipole-like expansion, without suffering the divergence problems of the ordinary multipole expansion.

In the usual approach to the calculation of dispersion energies, the interaction potential is expanded in a power series in R^{-n}:

$$V = \sum_{n=6}^{\infty} V_n R^{-n} \tag{1}$$

Here, the V_n are products of multipole operators of the separated fragments, such that $n = 2(l_a + l_b + 1)$ with l_a (l_b) taken to be the angular momentum quantum number of fragment A (B). By the use of second-order perturbation theory the expression for the dispersion interaction energy obtains

$$\Delta E_{disp} = \sum_{n=6}^{\infty} C_n R^{-n} \tag{2}$$

Here the C_n's are the familar van der Waals coefficients which are independent of R, the interfragment distance. While correct asymptotically, this expression increasingly overestimates the magnitude of the interaction energy for small R, where the charge cloud overlap becomes significant. The KNS method uses a Fourier transform of the nonexpanded interaction potential r_{ij}^{-1}, expressed in terms of the 2^l-pole polarizabilities which are functions of the wave vector k. Thus, it avoids the convergence problems of the ordinary multipole expansion given in eq 2. In the KNS method, the dispersion energy, E_{dd}, can be expressed as a *convergent* multipole-like expansion containing damping functions χ:

$$E_{dd} = -\sum_{l_a,l_b} C(l_a,l_b)\, \chi(l_a,l_b;R) R^{-2(l_a+l_b+1)} \tag{3}$$

the l_a and l_b refer to the 2^l-pole interactions of atoms A and B, respectively. Thus, the familiar van der Waals C_6 coefficient corresponds to $C(1,1)$ (or the induced dipole–induced dipole interaction), the C_8 coefficient to the sum of $C(1,2)$ and $C(2,1)$, and the C_{10} coefficient to the sum of $C(1,3)$, $C(3,1)$, and $C(2,2)$, and so forth. Note that each of the separate $C(l_a,l_b)$ coefficients has its own distinct damping function. This is in contrast to several semiempirical methods[6] for calculating the damped dispersion energies which assume single damping functions for each C_n value.

A typical set of damping functions, i.e., the χ of eq 3 (for the heteronuclear molecule NaAr), is shown in Figure 1. Note that they all approach unity at large R. The χ's approach zero at small R faster than does R^n. Thus the dispersion energies calculated by the present scheme have the correct limiting behavior at both large and small interfragment separations.

To date, KNS have applied their method to the calculation of potential curves for the ground states of the homonuclear rare gas diatomics He_2, Ar_2, and Xe_2[1-3] and to the ground state of Pb–rare gas molecules.[4] KNS find dissociation energies in reasonable agreement with those obtained from large scale ab initio calculations. This agreement is essentially exact for He_2 and within about 25% for Ar_2 and Xe_2. However, the accuracy of the method should depend more or less inversely on the degree to which the charge distributions of the atoms overlap. Thus the KNS scheme should work best for the light rare gases where this overlap is not large.

We have chosen to test the method more severely on systems where a large degree of charge cloud overlap is expected. The alkali atoms are highly polarizable; i.e. their charge distributions are very diffuse, and so they will overlap significantly even at large internuclear separations. Therefore, the alkali diatomic molecules are probably a "worst-case" test of the KNS approach. We also examine a mixed alkali–rare gas diatomic (a system of intermediate overlap) and an alkali diatomic cation (for which the charge cloud overlap should be negligible).

† Present Address: Harvard-Smithsonian Center for Astrophysics, 60 Garden St., Cambridge, MA 02138.

(1) M. Krauss, D. B. Neumann, and W. J. Stevens, *Chem. Phys. Lett.*, **66**, 29 (1979).
(2) M. Krauss, W. J. Stevens, and D. B. Neumann, *Chem. Phys. Lett.*, **71**, 500 (1980).
(3) M. Krauss and W. J. Stevens, *Chem. Phys. Lett.*, **85**, 423 (1982).
(4) H. Basch, P. S. Julienne, M. Krauss, and M. E. Rosenkrantz, *J. Chem. Phys.*, **73**, 6247 (1980).
(5) A. Koide, *J. Phys. B*, **9**, 3173 (1976).
(6) A. J. C. Varandas and J. Brandão, *Mol. Phys.*, **45**, 857 (1982).

0022-3654/85/2089-2804$01.50/0